Steady-State Flux and Lag Time in the Stratum Corneum Lipid Pathway: Results from Finite Element Models

H. FREDERICK FRASCH, ANA M. BARBERO

Health Effects Laboratory Division, National Institute for Occupational Safety and Health, 1095 Willowdale Road, Morgantown, West Virginia 26505

Received 14 February 2003; revised 29 April 2003; accepted 1 May 2003

ABSTRACT: Finite element model (FEM) solutions of the diffusion through two-dimensional representations of the stratum corneum (SC) lipid pathway are presented. Both simplified, regular "brick and mortar" models and a more complex, irregular model are analyzed. It is assumed that diffusion occurs only within the SC lipids and the lipids are isotropic. The steady-state flux and lag time are solved and compared with the corresponding values for a homogeneous membrane of the same thickness consisting of lipid material. Results confirm that the heterogeneous SC model behaves like a homogeneous membrane, meaning that FEM diffusion simulations are well approximated by an appropriate solution of the diffusion equation for a homogeneous membrane. Additionally, both steady-state flux and lag time (relative to these values in a homogeneous membrane) can be predicted from algebraic equations based on simple dimensionless descriptors of SC geometry. However, values for diffusivity derived from homogeneous membrane approximations to the FEM solutions (effective diffusivity, D^*) are not equal to the intrinsic diffusivity of the chemical in lipid. Furthermore, the pathlength derived from homogeneous membrane approximations to FEM solutions (effective pathlength, l^*) is not equal to the lipid pathlength and is not dependent on SC tortuosity. Whereas l^* is not a function of corneocyte overlap, D^* is. These model results suggest that diffusion properties of the SC lipid pathway can be correlated to SC geometry, but intrinsic diffusion coefficients and SC tortuosity cannot be derived from common diffusion cell experiments. Use of the model equations to predict permeability and lag time of lipophilic solutes is described. J Pharm Sci 92:2196–2207, 2003

Keywords: diffusion; mathematical model; percutaneous; skin; transdermal; permeability; lag time

INTRODUCTION

The diffusive flux of a permeant across a concentration gradient within a medium depends on its molecular mobility within the medium (diffusivity D) and on the geometry of the diffusion pathway. For a homogeneous membrane, the diffusional pathlength is simply the thickness of the membrane.

The stratum corneum (SC) is the thin ($\approx$10–20 μm), outermost layer of skin and is the primary permeation impediment of the skin barrier. The SC is not a homogeneous membrane; rather it is a biphasic arrangement of corneocytes—keratinized cellular remnants of epithelial differentiation—interposed with intercellular lipid lamellae. The lipid lamellae form a continuous pathway for diffusion through the SC, and today it is believed by many that this tortuous lipid path is the primary route of chemical permeation. Direct microscopic observation of model permeant localized primarily within the intercellular lipids,[1] as well as indirect evidence from biophysical

Correspondence to: H. Frederick Frasch (Telephone: 304-285-5755; Fax: 304-285-6041; E-mail: hbf9@cdc.gov)

Journal of Pharmaceutical Sciences, Vol. 92, 2196–2207 (2003)

measurements,[2] support this hypothesis; however, it should be recognized that little direct evidence exists to confirm or refute it.

Despite the geometric complexity of the SC lipid pathway, a number of investigators have demonstrated that the SC displays properties of a homogeneous membrane.[3] This means that results from SC diffusion experiments compare favorably with predictions of the diffusion equation for a homogeneous membrane, using appropriately fitted parameters. The purpose of this study was to investigate how the geometric arrangement of the SC lipid pathway determines its diffusion properties compared with the properties of a homogeneous membrane. We used a finite element modeling (FEM) approach to solve for diffusion through the lipid pathway of model SC structures, and compared results with the predictions of the diffusion equation for a homogeneous membrane. This approach yields values for steady-state flux and time lag as well as values of the parameters that comprise these quantities. Algebraic expressions that depend on dimensionless SC geometric descriptors were explored, for the prediction of both steady-state flux and lag time.

METHODS

SC Geometry

SC geometry is modeled in the simplest case as a two-dimensional "brick and mortar" structure (Fig. 1), where the diffusing substance is constrained to the "mortar." The upper and lower surfaces are not considered part of the diffusion path. The membrane consists of N layers of corneocytes; the width of corneocytes is d and their thickness is h. The lipid lamella are of thickness g in the horizontal direction and s in the vertical.

Several dimensionless parameters characterize the geometry of this structure. Following Cussler et al.,[4] the corneocyte aspect ratio is defined as $\alpha = d/h$ and the slit shape is given by $\sigma = s/h$. For $s \ll d$, the fractional volume loading of corneocytes is approximated by $\phi = h/(h+g)$. Following Johnson et al.,[5] the corneocyte offset ratio is quantified by $\omega = l_L/l_S$, where l_L is the length of the longest overlapping lipid path and l_S is the length of the shortest overlapping section (Fig. 1B). It follows that $l_L + l_S = d + s$. ω ranges from 1 for the complete overlap "brick and mortar" model of Figure 1A to ∞ for the case where no overlap occurs.

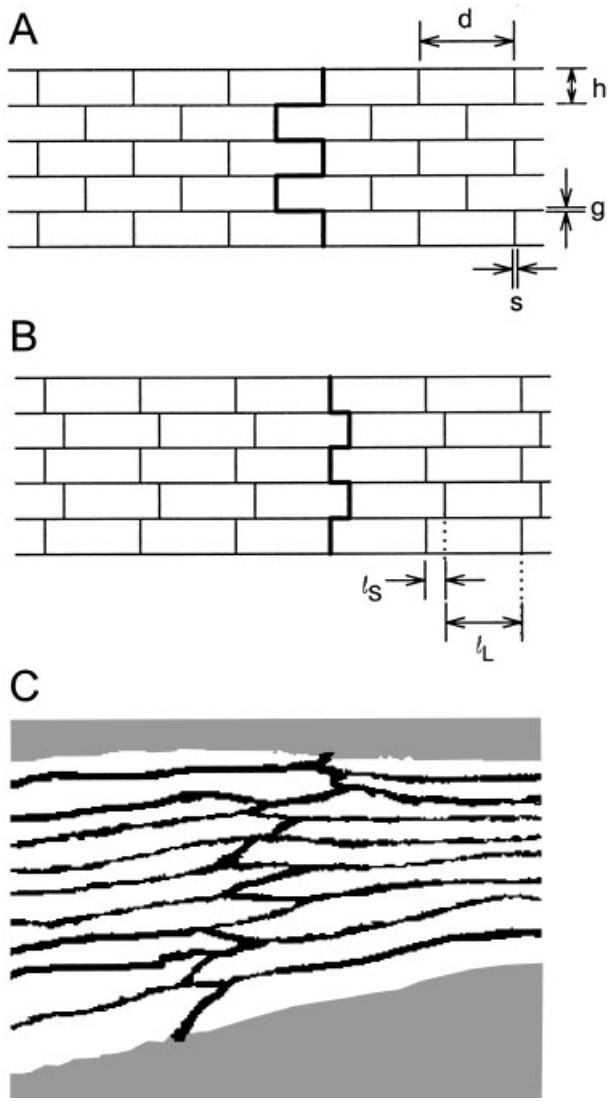

Figure 1. Geometric models of SC. Diffusion is constrained within the lipid layers, and the top and bottom surfaces are not considered part of the diffusion pathway. (A) Simple brick and mortar model,[15] with corneocytes analogous to bricks and lipid analogous to mortar. Corneocyte dimensions are quantified by d and h; lipid dimensions by g and s. Lipid pathlength is shown as the thicker path through the membrane. (B) Staggered brick and mortar model is generalized by introducing a variable corneocyte offset ratio ω, defined as the ratio of the longest overlapping section to the shortest overlapping section (l_L/l_S). Panel (A) then is the special case where $\omega = 1$. Lipid pathlength is shown as the thicker path through the membrane. (C). More realistic SC rendering, freely adapted from Schätzlein and Cevc's[11] study based on measurements from alkaline-expanded mouse skin.

The membrane thickness is given by $l_0 = Nh + (N-1)g$; for a membrane comprised of many layers, l_0 is approximated by $N(h+g)$. The lipid pathlength is shown graphically as the total length of the thick line pathway in Figure 1A and B, and is calculated by $l_{lip} = l_0 + (N-1)l_S$. Geometric tortuosity is defined[6] as $\tau_g = l_{lip}/l_0$. For a many-layered membrane and $s \ll d$, $\tau_g \approx 1 + \alpha\phi/(1+\omega)$.

For results presented here, we use realistic SC values of $N = 20$, $h = 1$ μm and $g = s = 0.1$ μm. Thus $l_0 = 21.9$ μm. These values were derived from a number of sources and include measurements made from mouse[7,8] and human[7,9,10] SC. ω is varied from 1 to ∞ and d from 20 to 60 μm to span reported values for human SC. For typical human SC, we take $\alpha = 40$ (corresponding to $d = 40$ μm) and $\omega = 3$ (based on Talreja et al.'s[6] estimate of average τ_g for non-expanded human SC). To simulate corneocyte swelling, we examined several cases for $h = 5$ μm.[6] To further investigate effects of SC geometry on flux and lag time, we examined several cases for $g = s = 0.5$ μm.

Geometric Descriptors of Irregular SC

To investigate the applicability of these geometric descriptors to a more realistic, irregular SC structure, we analyzed the rendering of a transverse section of SC shown in Figure 1C, derived from hairless mouse skin after alkaline expansion, and freely adapted from Schätzlein and Cevc.[11]

Statistical estimates of α, σ, ϕ, and ω of the mouse SC (Fig. 1C) were averaged from independent measurements made by two individuals (A.M.B. and H.F.F.) from digitized images using systematic sampling methods.[12] The pixel was used as the length unit. Figure 1C is 135 pixels wide and the total area of lipids + corneocytes is 10,181 square pixels. The image was divided into 10 equal horizontal sections of length Δx. A random number r between 0 an Δx was generated; then 10 vertical lines were placed over the image, beginning at distance r from the left edge and equally spaced Δx apart. The thickness of each corneocyte and each lipid layer intersecting the 10 vertical lines were measured; their average gave h and g respectively. We assumed $s = g$. Corneocyte length d was measured as the total width of Figure 1C (135 pixels) minus s. Volume ratio ϕ was measured as the ratio of the total number of square pixels comprising corneocytes to total number of square pixels comprising both corneocytes + lipids. The average of the lengths of the 10 vertical lines that intersect the SC was taken as l_0. The lipid pathlength l_{lip} was measured as the sum of the lengths of many small line segments making a contiguous path between the upper and lower surfaces, placed by judgment of the analyst. Offset ratio was then calculated from $\omega = \alpha\phi/(\tau_g - 1) - 1$.

Finite Element Models

A commercial finite element program (ANSYS 6.0, ANSYS Inc.) was used. The lipid layers of two-dimensional SC geometries were meshed with quadrilateral (0.05×0.05 μm), four-node elements with one degree of freedom (concentration) at each node. A diffusion coefficient D_0 within lipids is imposed, and it is assumed that the lipids are homogeneous and isotropic—there is no difference between lateral and transverse diffusivity. Whereas the complete overlap ($\omega = 1$) and no overlap ($\omega = \infty$) models exhibit lateral symmetry, the staggered overlap models (e.g., Fig. 1B) have periodicity. Periodic boundary conditions were applied using constraint equations: the concentrations at corresponding locations at the right edge and left edges of the lipid layers are constrained to be equal for all times. This constraint means that the membrane is treated as being infinitely repeating.

Steady-state and transient solutions of the diffusion through these model SC lipid bilayers were sought, with initial and boundary conditions imposed to mimic *in vitro* diffusion cell experiments. That is, the membrane was initially at zero concentration throughout. At time zero, a constant concentration difference was imposed across the membrane whereas the surface through which diffusing substance emerges was maintained at zero concentration. A sample ANSYS input program is available (see Supporting Information).

To demonstrate the use of this modeling approach using a more realistic, irregular SC geometry, we also developed an FEM based on the rendering of a transverse section of expanded mouse SC shown in Figure 1C. Here, the mesh size was 1 pixel × 1 pixel; lipids were again assumed homogeneous and isotropic; and identical initial and boundary conditions were imposed, including periodicity.

Regression Analysis

For the accumulation of mass of permeant per unit area over time [$Q(t)$] under the initial and

boundary conditions imposed on the finite element models with a concentration difference C maintained between the two surfaces, the analytical solution for a homogeneous membrane of thickness l is given by[13]:

$$Q(t) = Cl\left[\frac{Dt}{l^2} - \frac{1}{6} - \frac{2}{\pi^2}\sum_{n=1}^{\infty}\frac{(-1)^n}{n^2}\exp\left(\frac{-Dt}{l^2}n^2\pi^2\right)\right] \quad (1)$$

Finite element model results are fitted to eq. (1) by nonlinear regression using SigmaPlot 2001 (SPSS Inc.), which uses a Marquardt-Levenberg algorithm. The equation is truncated to 10 terms of the series. Results give estimates for the parameters effective diffusivity (D^*) and effective pathlength (l^*) and provide statistics relating to goodness of fit and variance of the parameters. Thus, D^* and l^* can be thought of as the diffusivity and thickness of a homogeneous membrane having the same permeability per unit area and lag time as the heterogeneous SC lipid pathway.

For consistency in analysis of FEMs, the FEM simulation time for all regressions was $\sim 10l^{*2}/(6D^*)$, and the maximum time step between FEM calculated values was set at $\sim 0.5l^{*2}/(6D^*)$.

The FEM and regression approach was checked by comparing results from a finite element model of a homogeneous membrane with the analytical solution expressed by eq. (1). The errors in estimation of D and l were $<1\%$. An alternate equation for flux[14] [the derivative of eq. (1)], which converges more rapidly for small times than eq. (1), was also tested. No significant differences in the values for D^* and l^* were found.

Estimates of Flux and Lag Time from SC Geometry

The total steady-state flux (units: mass/time) through a homogeneous membrane of area A_0 and thickness l_0, with concentration difference C maintained between the two surfaces, is given by

$$J_0 = CD_0A_0/l_0 \quad (2)$$

The barrier properties of such a membrane are characterized by the steady-state flux and by the lag time,

$$t_{\text{lag}0} = l_0^2/(6D_0) \quad (3)$$

The analyses presented herein do not consider any partitioning between membrane and surrounding vehicle.

Several estimates for flux of permeant confined to the SC lipid path (J^*) have been reported, based on SC geometry. The approach exemplified by Michaels et al.[15] and Moghimi et al.[16]considers the reduction in SC surface area normal to the flux and the increased tortuous lipid pathlength. For example, Moghimi et al.'s eq. (6)[16] can be written as:

$$\frac{J_0}{J^*} = \frac{A_0\tau}{A^*} \approx \frac{\alpha}{\sigma}\left(1 + \frac{\alpha\phi}{1+\omega}\right) \quad (4)$$

with $A_0/A^* \approx \alpha/\sigma$. Michaels et al.'s eq. (22)[15] follows a similar line of reasoning for the special case of complete corneocyte overlap ($\omega = 1$).

Cussler's group[4] derived the following expression:

$$\frac{J_0}{J^*} = 1 + \frac{\alpha\phi}{\sigma} + \frac{\alpha^2\phi^2}{4(1-\phi)} \quad (5)$$

Equation (5) accounts in detail for the reduction in area along the entire permeation pathway as well as the increase in effective pathlength of the lipid pathway. The first term (unity) represents the limiting case of a homogeneous membrane, where volume loading ϕ is zero (no corneocytes). The second term represents the resistance of the short vertical lipid slits between corneocytes in the same horizontal plane, and the third term accounts for resistance to diffusion of the tortuous path around the corneocytes. See Cussler et al.[4] for a complete derivation.

Cussler et al.'s analysis, which was not specifically related to skin, applies to the special case corresponding to complete corneocyte overlap (Fig. 1A). Johnson et al.[5] derived a factor to account for variable ω:

$$\frac{J_0}{J^*} = 1 + \frac{\alpha\phi}{\sigma} + \frac{\omega}{(1+\omega)^2}\frac{\alpha^2\phi^2}{(1-\phi)} \quad (6)$$

Geometry-based expressions for lag time in the SC lipid pathway have also been reported. Both Flynn et al.[17] and Moghimi et al.[16] have suggested the following:

$$\frac{t_{\text{lag}^*}}{t_{\text{lag}0}} = \tau^2 \approx \left(1 + \frac{\alpha\phi}{1+\omega}\right)^2 \quad (7)$$

whereas Cussler's group[18,19] propounds:

$$\frac{t_{\text{lag}^*}}{t_{\text{lag}0}} = 1 + \left(\frac{\alpha\phi}{2}\right)^2 \quad (8)$$

A new expression is proposed here. It is useful to consider the components of the ratio J_0/J^* for the SC lipid pathway:

$$\frac{J_0}{J^*} = \frac{D_0}{l_0}\frac{l^*}{D^*}\frac{A_0}{A^*} \tag{9}$$

The effective pathlength l^* is dominated by the lateral lipid pathways. Within each horizontal layer, transient diffusion occurs laterally to fill the lipid lamellae. This lateral membrane capacity significantly contributes to the observed lag time. Hence, it seems reasonable to assert that effective pathlength can be approximated by $l^* = N(d+h+g)$. This assertion will be tested later (Results). Multiplying eq. (9) by $l^*/l_0 \approx 1+\alpha\phi$, rearranging and substituting eq. (6), lag time $[t_{lag^*} = l^{*2}/(6D^*)]$ can be expressed in terms of the geometric descriptors:

$$\frac{t_{lag^*}}{t_{lag0}} = \frac{\sigma(1+\alpha\phi)}{\alpha}\left(1+\frac{\alpha\phi}{\alpha}+\frac{\omega}{(1+\omega)^2}\frac{\alpha^2\phi^2}{(1-\phi)}\right) \tag{10}$$

Finite Element Results Compared with Geometric Estimates

Values for the parameters l^* and D^*, derived from nonlinear regression of FEM model results with eq. (1), are used in eq. (9) to compare with the predictions of eqs. (4)–(6). FEM lag times calculated from $l^{*2}/(6D^*)$ are compared with the predictions of eqs. (7), (8), and (10).

RESULTS

Measured geometric descriptors of the SC membrane in Figure 1C are: $\alpha = 22$; $\sigma = 0.33$; $\phi = 0.77$; $\omega = 10$. We note that these values have been derived from a rendering based on alkaline-expanded mouse SC, and do not apply to normal human SC.

Figure 2 displays typical finite element model results for the diffusion simulations, along with best-fit regression estimates using eq. (1). For all simulations tested, the correlation coefficient (R^2) exceeded 0.999. Estimates of the coefficients D^* and l^* were all highly significant ($p < 0.0001$), with the largest coefficient of variation 2.4% of the estimated value.

Figure 3 shows values for D^* and l^* for FEM simulations that were performed using the brick and mortar and staggered brick and mortar models. For clarity, values of $\omega > 20$ are not displayed, although simulations were performed for ω up to ∞ (corresponding to no corneocyte overlap).

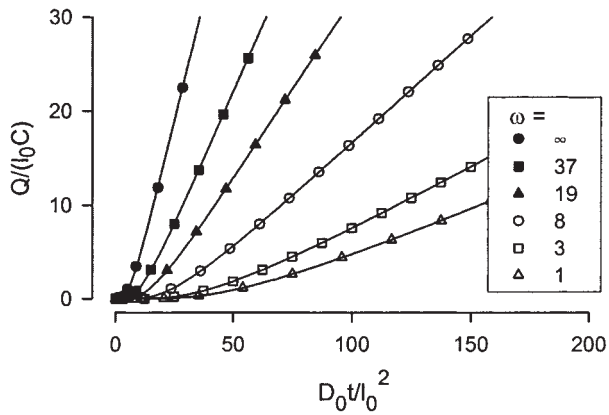

Figure 2. Typical FEM results for diffusion simulations (symbols), along with best-fit regression estimates using eq. (1) (lines). Shown are simulations for $\alpha = 40$, $\sigma = 0.1$, $\phi = 0.91$, and ω ranging from 1 to ∞. In all cases, the correlation coefficient (R^2) between FEM results and eq. (1) exceeds 0.999.

Figure 4 displays FEM-derived values of steady-state flux [eq. (9)] compared with the predictions of eq. (4) (Fig. 4A) and eq. (5) (Fig. 4B). For clarity, not all FEM simulations are presented. For a given value of α, arrows indicate the direction of increasing ω, ranging from 1 to ∞.

Figure 5 displays FEM predictions of lag time compared with the predictions of eq. (7) (Fig. 5A) and eq. (8) (Fig. 5B). For clarity, not all FEM simulations are presented. For a given value of α, arrows indicate the direction of increasing ω, ranging from 1 to ∞.

Figure 6A shows FEM-derived values for l^* in comparison with the expression $N(d+h+g)$. Figure 6B shows steady-state flux from FEM models compared with the predictions of eq. (6). Figure 6C displays FEM lag time in comparison with the predictions of eq. (10). All FEM simulations are shown.

DISCUSSION

Summary

We have presented results from finite element models to characterize diffusion through SC

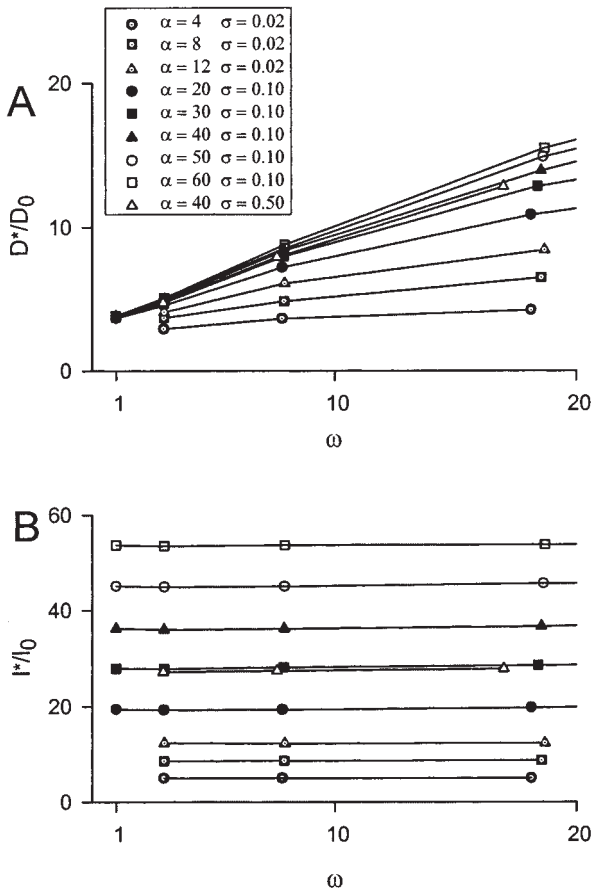

Figure 3. Model SC diffusion transport parameters. Values for effective SC diffusivity (D^*) (A) and effective SC diffusional pathlength (l^*) (B) derived from regression of FEM simulations with eq. (1). For clarity, not all FEM simulations of brick and mortar models are shown. For $\sigma = 0.02$, $\phi = 0.98$; for $\sigma = 0.1$, $\phi = 0.91$; for $\sigma = 0.5$, $\phi = 0.67$.

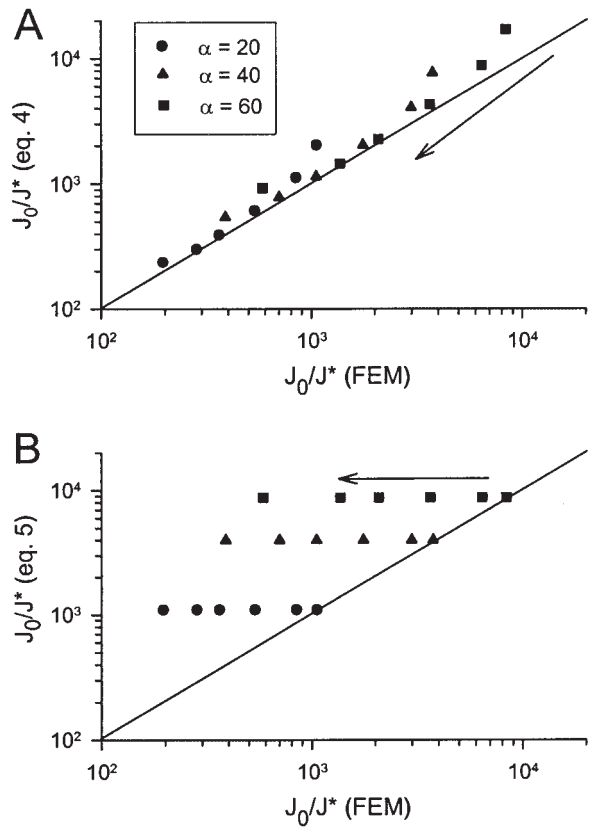

Figure 4. Model SC steady-state flux compared with geometric estimates. FEM-derived values of steady-state flux [eq. (9)] compared with the predictions of eq. (4) (A) and eq. (5) (B). The line of identity is also displayed in both panels. For clarity, not all FEM simulations are presented. For a given value of α, arrows indicate direction of increasing ω, ranging from 1 to ∞.

lipids and to investigate effects of SC structural organization. Although this approach was recently undertaken by Heisig et al.,[20] the analyses presented herein are unique. Conditions that mimic common diffusion cell experiments are modeled, and results are compared with appropriate analytical solutions to the diffusion equation for a homogeneous membrane. This comparison gives estimates of apparent diffusivity and apparent pathlength of these two-dimensional models. We found that the model SC lipid pathway exhibits characteristics of a homogeneous membrane, and both steady-state flux and lag time can be estimated from knowledge of the SC geometry, along with knowledge of the transport properties within the lipid phase. However, the effective diffusional pathlength cannot be defined as the lipid pathlength, and the effective diffusion coefficient differs from the intrinsic diffusion coefficient. These results imply that neither intrinsic diffusivity nor SC tortuosity can be deduced using common diffusion cell experiments.

The SC as a Pseudo-Homogeneous Membrane

Results from our finite element models of the SC confirm what has been demonstrated experimentally[3]: the SC "behaves" like a homogeneous membrane for diffusion. This is demonstrated by Figure 2, which shows FEM simulated diffusion in comparison with the corresponding solution of the diffusion equation for a homogeneous

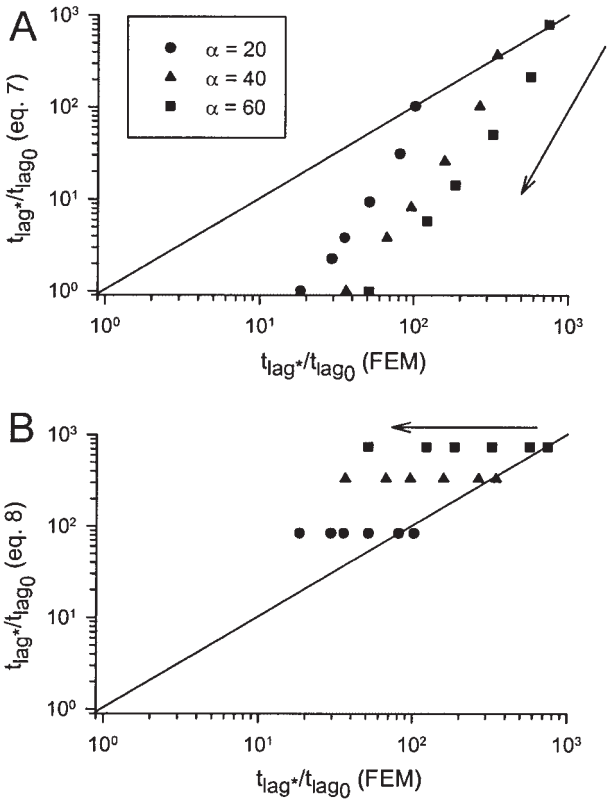

Figure 5. Model SC lag time compared with geometric estimates. FEM-derived values of lag time [$l^{*2}/(6D^*)$] compared with the predictions of eq. (7) (A) and eq. (8) (B). The line of identity is also displayed in both (A) and (B). For clarity, not all FEM simulations are presented. For a given value of α, arrows indicate direction of increasing ω, ranging from 1 to ∞.

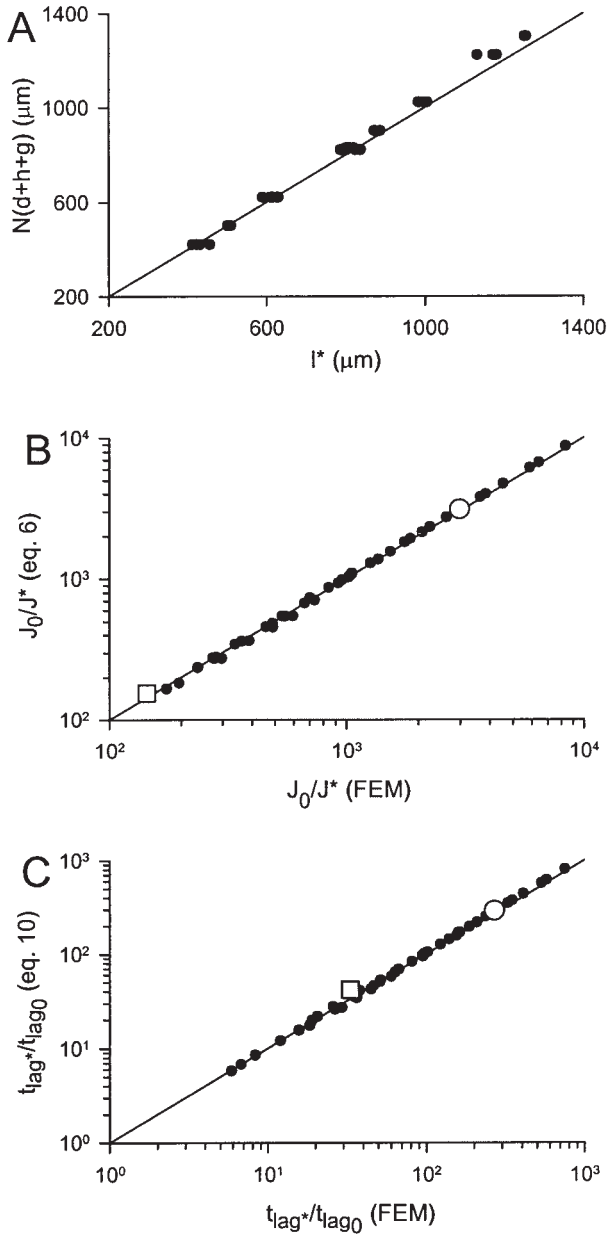

Figure 6. Model SC barrier properties compared with geometric estimates. (A) FEM-derived values for l^* in comparison with the expression $N(d+h+g)$. (B) Steady-state flux from FEM models compared with the predictions of eq. (6). (C) FEM estimates of lag time in comparison with the predictions of eq. (10). The line of identity is displayed in all panels. All FEM simulations are shown. In (B) and (C): open circles indicate the results derived from reported values of geometric descriptors for human SC: $\alpha = 40$; $\sigma = 0.1$; $\phi = 0.91$; $\omega = 3$. Open squares represent the values derived from the SC rendering of Figure 1C.

membrane. Results also confirm the enormous contribution of SC geometry to SC barrier properties. Using geometric values derived from human SC, the model SC membrane is ~3000 times less permeable than a homogeneous membrane made of the same lipid material (Fig. 6B, open circles), and its lag time is ~300 times longer (Fig. 6C, open circles).

Steady-State Flux in SC Models

The most significant finding of this study is that both steady-state flux and diffusional time lag can be predicted based on dimensionless geometric descriptors of the SC. This is verified for both the simplified SC geometries of Figure 1A and B, as well for one case of a more realistic geometry (Fig. 1C). Results support the use of eq. (6) to

predict steady-state flux and eq. (10) to predict time lag. Although the full range of values for all variables (α, σ; ϕ, and ω) was not tested, a wide range that fully spans reported values for normal and swollen SC was examined.

Figure 6B displays excellent correlation between the FEM-derived values of steady-state flux and the predictions of eq. (6). Neither eq. (4) nor eq. (5) display the same level of correlation (Fig. 4). Equation (4) fails because, although it accounts for the reduction in cross-sectional area available for diffusion at the surfaces of the membrane, it does not take into consideration the diffusion areas along the entire permeation pathway. (The equation derived by Michaels et al.[15] is similar to eq. (4), but slightly more complex in that Michaels et al. appear to consider the SC surface of a three-dimensional structure with a two-dimensional lipid pathway.) Equation (5) correctly accounts for different areas for diffusion along the entire pathway but fails because it does not consider corneocyte overlap. This equation, derived by Cussler et al.,[4] was applied to artificial barrier membranes containing selective impermeable flakes and has undergone experimental verification.[19] In applying this analysis to the SC, Johnson et al.[5] derived the dependence of flux on ω and presented a form of eq. (6), which reduces to eq. (5) for the special case of $\omega = 1$. The results presented here verify the use of eq. (6) for the prediction of steady-state flux and permeability.

Lag Time in SC Models

No previous expression known to the authors was able to adequately predict lag time on the basis of geometric descriptors. Previous expressions[16–19] fail because of incorrect assumptions regarding what constitutes effective diffusivity and effective pathlength (see Appendix). The FEM results presented here suggest an alternate approach. An appropriate expression for l^* has been developed and confirmed by the FEM model results (Fig. 6A). Using this expression in eq. (9), along with the appropriate expression for J_0/J^* [eq. (6)], creates a new formula for time lag in the SC lipid pathway. Equation (10) exhibits excellent correlation with the lag time derived from the FEM models (Fig. 6C).

For $\omega = 1$, both eqs. (7) and (8) adequately predict the FEM lag times (Fig. 5). This can be understood by simplifying eq. (10) for conditions that generally hold for the SC. In making the approximation $(1 + \alpha\phi)/\alpha \approx \phi$ (valid for $\alpha\phi \gg 1$), and noting that $\sigma\phi/(1 - \phi) = 1$ (for $s = g$), eq. (10) reduces to

$$\frac{t_{\text{lag}^*}}{t_{\text{lag0}}} = \sigma\phi + \alpha\phi^2 + \frac{\omega}{(1+\omega)^2}\alpha^2\phi^2 \qquad (11)$$

With $\omega = 1$, this is very close to both eqs. (7) and (8), because the second order terms dominate.

Effective Pathlength in SC Models

It is noteworthy that the effective pathlength l^* derived from the FEM models is independent of corneocyte overlap (Fig. 3B). In other words, effective pathlength does not depend on lipid tortuosity but rather is well predicted by the expression $N(d + h + g)$ (Fig. 6A), so that the ratio $l^*/l_0 \approx 1 + \alpha\phi$. This can be understood by considering transient diffusion within the lipid lamellae. Until the steady state is reached, a concentration gradient develops along the lateral lipid layers that produces a net flux of permeant: there is initially zero concentration within the lateral layers, and as permeant diffuses downward from the surface, a non-zero concentration exists at the intersection of the vertical slits and the lateral paths. A concentration gradient develops along both sides of a vertical slit until net permeant flux from the two vertical slits on either side of it eliminates the gradient—resulting in no further net flux. Thus, this lateral membrane capacity contributes to the overall effective diffusional pathlength. The total lateral component of l^* is then given by $(N - 1)d$ whereas the vertical component is identical to l_0. Therefore $l^* = (N - 1)(d + g) + Nh \approx N(d + h + g)$.

This is not to say that time lag does not depend on corneocyte overlap. Both steady-state flux [eq. (6)] and time lag [eq. (10)] are functions of ω. This dependence is captured in the FEM-derived values for D^*. (An expression for D^* can be obtained from eqs. (9) and (6), substituting the expressions for l^* and for A_0/A^* given previously.)

Significance of Results

The significance of these results is underscored by recent theoretical[21–23] and experimental[2,24–27] investigations of the kinetics of percutaneous absorption. Appropriate values for both effective diffusivity and effective pathlength are required to calculate time-dependent skin diffusion phenomena such as time lag, membrane desorption,

finite dosing, short-term exposures, and repeated drug dosing. Experimental estimates of diffusion coefficients and pathlengths have been made from combined steady-state and non-steady-state diffusion measurements in isolated SC and epidermal membranes.[2,25,26] The analysis of Bunge et al.[28] demonstrates some of the pitfalls encountered if, for example, no consideration is given to the reduction in cross-sectional area available for diffusion. The results presented here suggest further pitfalls, even if cross-sectional area is considered: the diffusion coefficients derived from experimental results cannot be directly related to intrinsic diffusion coefficients, and the pathlength derived from experimental results is not a function of SC tortuosity. Potts and Francoeur[2] estimated a diffusional pathlength of ~50 times greater than SC thickness for water vapor diffusion. (Whether this value holds for more lipophilic substances is not known.) Although it is difficult to postulate an SC tortuosity of 50 (reasonable values[6] are close to 10), 50 is close to the value of 36 for l^*/l_0 predicted by the FEM model for human SC values (Fig. 3B; $\alpha = 40$, $\sigma = 0.1$).

Application of Model Equations to Predict Permeability and Lag Time of a Permeant

The equations presented here can be used to predict permeability and lag time of a given solute in the SC. For solutes that diffuse solely within the lipid phase of the SC, the steady-state permeability coefficient is given by:

$$k_p = K_{L\_V}\frac{D^*}{l^*}\frac{A^*}{A_0} = K_{L\_V}\frac{J^*}{J_0}\frac{D_0}{l_0} \qquad (12)$$

where K_{L_V} is the equilibrium partition coefficient between the lipid fraction of the SC and the surrounding vehicle. Note that this differs from the more commonly reported SC-vehicle partition coefficient, which represents the bulk distribution of solute between the total volume of SC and vehicle:

$$K_{L\_V} = \frac{K_{SC\_V}}{1-\phi} \qquad (13)$$

Therefore, permeability can be predicted based on knowledge of SC geometry, with the ratio J^*/J_0 given by eq. (6), and on the diffusion coefficient of the permeant in lipids. Reasonable values for SC geometry are given in the text. Johnson et al.[29] measured lateral diffusion coefficients in lipids extracted from human SC. Using the fluorescence recovery after photobleaching method, they report molecular weight (MW)-dependent diffusivities of several lipophilic fluorescent probes ranging from 3.06×10^{-9} to 2.34×10^{-8} cm^2/s, for MW of 629 and 223 Da, respectively. Additionally, the authors report a two-parameter empirical equation that nicely correlates diffusivity as a function of MW.

Lag time for diffusion within the SC lipids can also be predicted from SC geometry and knowledge of D_0. For a given solute, t_{lag^*} can be obtained by multiplying the right-hand side of eq. (10) by $l_0^2/(6D_0)$, with D_0 again estimated from the results of Johnson et al.[29]

Model Limitations and Conclusions

In the models presented here, we impose the conditions that diffusion occurs only within lipid bilayers and that diffusivity within the lipids is isotropic. These simplifications are model limitations but may be acceptable if, as postulated by Johnson et al.,[5] lateral lipid bilayer diffusion is the primary permeation pathway in the SC. Mitragotri[30] recently described four possible permeation pathways with lateral lipid transport taking a less prominent role; however, little direct experimental evidence exists in support of a particular transport mechanism in skin. Model results presented here are valid only for the lateral lipid bilayer diffusion pathway.

In conclusion, we have presented results from two-dimensional FEM models for diffusion within lipid bilayers of SC membranes. The results demonstrate important implications about the effective diffusional pathlength and effective diffusivity within the SC. Although the exact relationship between parameters of the SC geometry and estimates of steady-state flux and lag time may differ for a more realistic SC that has to be described as a three-dimensional structure, this work makes it reasonable to assume that those relationships can be determined with additional analysis.

SUPPORTING INFORMATION

Supporting material is available for this article at the following Web address: http://dx.doi.org/10.1002/jps.10466, or from the authors. It is a commented ANSYS input file that is used to generate and solve a finite element model of diffusion through SC lipids conforming to a staggered brick and mortar geometry (Fig. 1B). Note that we use a

heat conduction-diffusion analogy (see Crank J. 1975. The mathematics of diffusion, 2nd ed. Oxford: Clarendon Press, pp 8–10).

APPENDIX

Further Discussion on Effective Diffusivity and Pathlength

Our use of the terms D^* and l^*—effective diffusivity and effective pathlength—differs somewhat from commonly used terms apparent diffusivity and apparent pathlength. Here, we explain the differences and why the "new" terms are appropriate. The problem with the terms as commonly defined is that they cannot be used to correctly predict both steady-state and transient diffusion phenomena.

In a tradition that extends over ~125 years since Maxwell, for diffusion within heterogeneous or composite media, an apparent diffusion coefficient (D') is used to incorporate the effects of geometry on the permeation of the diffusing compound.[31] As applied to the SC, D' is the diffusion coefficient that is postulated when the SC is treated as a pseudo-homogeneous membrane whose thickness is the same as the SC.[28]

Such an approach would be perfectly acceptable here if one were interested only in steady-state flux. If D' as defined here were used, then the ratio of steady-state flux in the homogeneous membrane to that in the SC is given by

$$\frac{J_0}{J^*} = \frac{D_0}{D'}\frac{A_0}{A^*} \tag{A.1}$$

Accordingly, an expression for D' can be developed in terms of our D^* and l^* [from eq. (9), main text]:

$$D' = D^*\frac{l_0}{l^*} \tag{A.2}$$

Use of this expression in eq. (A.1) would then satisfy the results of the finite element models, for the steady state.

However, if these concepts are applied to a calculation of lag time in the SC, we obtain:

$$t_{\text{lag}} = \frac{l_0^2}{6D'} = \frac{l_0 l^*}{6D^*} \neq t_{\text{lag}^*} \tag{A.3}$$

The lag time calculated from eq. (A.3) does not satisfy the results of the FEM. Therefore, the use of apparent diffusivity as it has been traditionally defined cannot simultaneously account for both steady-state and non-steady-state diffusion phenomena. If steady-state permeability is the sole interest, which has generally been the case in the traditional use of the concept, then the approach is perfectly acceptable.

Another common approach is to consider an apparent pathlength in the SC as equal to the lipid pathlength. The steady-state flux ratio is then given by:

$$\frac{J_0}{J^*} = \frac{D_0}{D''}\frac{l_{\text{lip}}}{l_0}\frac{A_0}{A^*} \tag{A.4}$$

D'' is still an apparent diffusion coefficient, but its value differs from D'. In order for eq. (A.4) to satisfy the FEM results for steady-state flux,

$$D'' = D^*\frac{l_{\text{lip}}}{l^*} \tag{A.5}$$

Applying these definitions to the calculation of lag time in the SC:

$$t_{\text{lag}} = \frac{l_{\text{lip}}^2}{6D''} = \frac{l_{\text{lip}} l^*}{6D^*} \neq t_{\text{lag}^*} \tag{A.6}$$

We run into the same problem as before: we cannot use the lipid pathlength to simultaneously account for both steady-state and non-steady-state phenomena.

A special case of the above approach is to consider both that apparent pathlength is equal to the lipid pathlength, and that apparent diffusivity is equal to the diffusivity within the lipid phase. For this case, eq. (4) (main text) results as the ratio of fluxes, and eq. (7) (main text) results to describe the ratio of lag times. The analyses described in the main text of this article demonstrate that these expressions fail.

Yet another approach has been taken, and that is to lump all effects of geometry into an "effective tortuosity"[5] as follows:

$$\frac{J_0}{J^*} = \tau_{\text{eff}} \tag{A.7}$$

Note that these authors use the term τ^*; however, we do not wish to confuse their terminology with ours. To satisfy the FEM results for steady-state flux, then,

$$\tau_{\text{eff}} = \frac{D_0}{D^*}\frac{l^*}{l_0}\frac{A_0}{A^*} \tag{A.8}$$

This concept has been applied to the calculation of a diffusional transport time for desorption from the SC.[26,32] This transport time equals $6 \times t_{\text{lag}}$.

Accordingly,

$$t_{lag} = \frac{(l_0 \tau_{eff})^2}{6D_0} = \frac{l^{*2} D_0}{6D^{*2}} \left(\frac{A_0}{A^*}\right)^2 \neq t_{lag^*} \qquad (A.9)$$

Thus, the concepts of apparent diffusivity and pathlength, as traditionally used, fail to account for both steady-state permeability and non-steady diffusion phenomena such as lag time, as predicted by the finite element models of the SC lipid pathway. In the present study, the concepts of effective diffusivity and effective pathlength are defined as the diffusivity and thickness of a homogeneous membrane, having the same permeability (per unit area) and lag time, as the SC lipid pathway. Used together, they are able to describe both steady-state and transient diffusion phenomena.

NOMENCLATURE

List of Abbreviations Used in Mathematical Development

A_0 area of homogeneous membrane surface normal to direction of flux
A^* area of lipid lamella at surface of membrane normal to direction of flux
C concentration
d corneocyte length
D diffusivity
D_0 intrinsic diffusivity; diffusivity within SC lipids
D^* effective diffusivity in a membrane where permeation occurs exclusively within lipid lamellar pathway
g lipid lamellar thickness in horizontal direction
h corneocyte thickness
J_0 total steady-state flux through a specified area of a homogeneous membrane
J^* total steady-state flux through a specified area of the exclusively lipid lamellar pathway
l diffusional pathlength
l_0 homogeneous membrane thickness; SC thickness
l^* effective SC pathlength, where permeation occurs exclusively within lipid lamellar pathway
l_{lip} length of SC lipid pathway
l_L length of long sections of lipid pathway associated with overlapping sections of corneocytes
l_S length of short sections of lipid pathway associated with overlapping sections of corneocytes
N number of corneocyte layers
Q mass of permeant per unit area
s lipid lamellar thickness in vertical direction
t time
t_{lag0} lag time for diffusion within homogeneous membrane
t_{lag^*} lag time for diffusion within the exclusively lipid pathway
α corneocyte aspect ratio $= d/h$
σ slit shape $= s/h$
τ_g geometric tortuosity of lipid pathway $= l_{lip}/l_0$
ϕ volume fraction of corneocytes
ω corneocyte offset ratio $= l_L/l_S$

REFERENCES

1. Bodde HE, van den Brink I, Koerten HK, de Haan FHN. 1991. Visualization of *in vitro* percutaneous penetration of mercuric chloride: Transport through intercellular space versus cellular uptake through desmosomes. J Control Release 15:227–236.
2. Potts RO, Francoeur ML. 1991. The influence of stratum corneum morphology on water permeability. J Invest Dermatol 96:495–499.
3. Kalia YN, Pirot F, Guy RH. 1996. Homogeneous transport in a heterogeneous membrane: Water diffusion across human stratum corneum *in vivo*. Biophys J 71:2692–2700.
4. Cussler EL, Hughes SE, Ward WJ III, Aris R. 1988. Barrier membranes. J Membr Sci 38:161–174.
5. Johnson ME, Blankschtein D, Langer R. 1997. Evaluation of solute permeation through the stratum corneum: Lateral bilayer diffusion as the primary transport mechanism. J Pharm Sci 86:1162–1172.
6. Talreja PS, Kasting GB, Kleene NK, Pickens WL, Wang T-F. 2001. Visualization of the lipid barrier and measurement of lipid pathlength in human stratum corneum. AAPS Pharm Sci 3(2): Article 13 (http://www.pharmsci.org).
7. Wildnauer RH, Miller DL, Humphries WT. 1975. A physicochemical approach to the characterization of stratum corneum. In: Baier RE, editor. Applied chemistry at protein interfaces. Washington DC: American Chemical Society, pp 74–124.
8. Menton DN. 1976. A minimum-surface mechanism to account for the organization of cells into columns in the mamallian epidermis. Am J Anat 145:1–21.
9. Mershon MM. 1975. Barrier surfaces of skin. In: Baier RE, editor. Applied chemistry at protein interfaces. Washington DC: American Chemical Society, pp 41–73.

10. Elias PM, Cooper ER, Korc A, Brown BE. 1981. Percutaneous transport in relation to stratum corneum structure and lipid composition. J Invest Dermatol 76:297–301.
11. Schätzlein A, Cevc G. 1998. Non-uniform cellular packing of the stratum corneum and permeability barrier function of intact skin: A high-resolution confocal laser scanning microscopy study using highly deformable vesicles (Transfersomes). Br J Dermatol 138:583–592.
12. Bolender RP, Pentcheff ND. 1992. Current methods in quantitative morphology. QM2000 Version 2.0. Seattle: University of Washington.
13. Crank J. 1975. The mathematics of diffusion, 2nd ed. Oxford: Clarendon Press, p 51.
14. Rogers WA, Buritz RS, Albert D. 1954. Diffusion coefficient, solubility, and permeability for helium in glass. J Appl Phys 25:868–875.
15. Michaels AS, Chandrasekaran SK, Shaw JE. 1975. Drug permeation through human skin: Theory and *in vitro* experimental measurement. AIChE J 21: 985–996.
16. Moghimi HR, Williams AC, Barry BW. 1996. A lamellar matrix model for stratum corneum intercellular lipids. II. Effect of geometry of the stratum corneum on permeation of model drugs 5-fluorouracil and oestradiol. Int J Pharm 131:117–129.
17. Flynn GL, Yalkowsky SH, Roseman TJ. 1974. Mass transport phenomena and models: Theoretical concepts. J Pharm Sci 63:479–510.
18. Perry D, Ward WJ, Cussler EL. 1989. Unsteady diffusion in barrier membranes. J Membr Sci 44:305–311.
19. Lape NK, Yang C, Cussler EL. 2002. Flake-filled reactive membranes. J Membr Sci 209:271–282.
20. Heisig M, Lieckfeldt R, Wittum G, Mazurkevich G, Lee G. 1996. Non steady-state descriptions of drug permeation through stratum corneum. I. The biphasic brick-and-mortar model. Pharm Res 13: 421–426.
21. Anissimov YG, Roberts MS. 1999. Diffusion modeling of percutaneous absorption kinetics I. Effects of flow rate, receptor sampling rate and viable epidermal resistance for a constant donor concentration. J Pharm Sci 88:1201–1209.
22. Anissimov YG, Roberts MS. 2001. Diffusion modeling of percutaneous absorption kinetics. II. Finite vehicle volume and solvent deposited solids. J Pharm Sci 90:504–520.
23. Kalia YN, Guy RH. 2002. Modeling transdermal drug release. Adv Drug Deliv Rev 48:159–172.
24. Roberts MS, Triggs EJ, Anderson RA. 1975. Permeability of solutes through biological membranes measured by a desorption technique. Nature 257: 225–227.
25. Pellett MA, Watkinson AC, Hadgraft J, Brain KR. 1997. Comparison of permeability data from traditional diffusion cells and ATR-FTIR spectroscopy. Part II. Determination of diffusional pathlengths in synthetic membranes and human stratum corneum. Int J Pharm 154:217–227.
26. Mitragotri S. 2000. *In situ* determination of partition and diffusion coefficients in the lipid bilayers of stratum corneum. Pharm Res 17:1026–1029.
27. Kasting GB. 2001. Kinetics of finite dose absorption through skin. I. Vanillylonanamide. J Pharm Sci 90:202–212.
28. Bunge AL, Guy RH, Hadgraft J. 1999. The determination of a diffusional pathlength through the stratum corneum. Int J Pharm 188:121–124.
29. Johnson ME, Berk DA, Blankschtein D, Golan DE, Jain RK, Langer RS. 1996. Lateral diffusion of small compounds in human stratum corneum and model lipid bilayer systems. Biophys J 71:2656–2668.
30. Mitragotri S. 2003. Modeling skin permeability to hydrophilic and hydrophobic solutes based on four permeation pathways. J Control Release 86: 69–92.
31. Crank J. 1975. The mathematics of diffusion, 2nd ed. Oxford: Clarendon Press, pp 266–285.
32. Mitragotri S. 2001. Effect of therapeutic ultrasound on partition and diffusion coefficients in human stratum corneum. J Control Release 71:23–29.